Journal of the Serbian Chemical Society
JSCS-info@shd.org.rs • www.shd.org.rs/JSCS
J. Serb. Chem. Soc. *90* (0) 1–14 (2025)
JSCS–13354
Original scientific paper
Published 15 Dec 2025

Development of a glass–ceramic composite reinforced with *β*-wollastonite synthesized *via* a hydrothermal method

MARJAN RANĐELOVIĆ[1]*, CHARLES C. SORRELL[2], SHARON KOPPKA[3], ALEKSANDRA ZARUBICA[1], MILAN Z. MOMČILOVIĆ[1] and DIRK ENKE[3]

[1]*University of Niš, Faculty of Sciences and Mathematics, Department of Chemistry, Višegradska 33, 18000 Niš, Serbia,* [2]*School of Materials Science and Engineering, University of New South Wales, Sydney NSW 2052, Australia and* [3]*Institute of Chemical Technology, University of Leipzig, Linne str. 3, 04103 Leipzig, Germany*

(Received 26 April, revised 20 May, accepted 25 August 2025)

Abstract: *β*-wollastonite (*β*-$CaSiO_3$) microfibres were successfully synthesized using a one-step, template-free hydrothermal reaction involving calcium nitrate and sodium metasilicate in an alkaline medium. The synthesis of microfibres was completed at 220 °C within only 240 min under an autogenous pressure of 19 bar (1.9 MPa). This method avoids the formation of xonotlite as an intermediate phase, eliminating the need for subsequent calcination to achieve wollastonite. X-ray diffraction (XRD) confirmed the *β*-wollastonite phase, while post-calcination analyses indicated enhanced crystallinity and structural characteristics. Scanning electron microscopy (SEM) revealed a needle-like morphology and N_2 adsorption-desorption analysis demonstrated a developed surface area of 26 m^2 g^{-1} with notable mesoporosity. These advantageous features facilitated the integration of *β*-wollastonite into the synthesis of a glass–ceramic composite, which was characterized for its morphological, structural, textural, and *in vitro* bioactivity properties. The composite was prepared by mixing *β*-wollastonite and bioactive glass powders in a 1:4 mass ratio, followed by compaction through uniaxial pressing and sintering at 1000 °C for various time intervals. For comparison, compacted pure bioactive glass samples were also sintered under identical conditions. Structural, morphological, textural and *in vitro* bioactivity characterizations demonstrated that the incorporation of *β*-wollastonite led to a more uniform and narrower pore size distribution and promoted neck formation between particles, indicating its potential for bone regeneration applications.

Keywords: sintering; bioceramics; mineral; mesoporosity.

* Corresponding author. E-mail: hemija@gmail.com
https://doi.org/10.2298/JSC250426072R

INTRODUCTION

Wollastonite is a naturally occurring mineral with the chemical formula $CaSiO_3$ and two polymorphic forms; the low-temperature phase β-wollastonite and the high-temperature phase α-wollastonite (pseudowollastonite).[1] It is a member of the inosilicates with a single-chain structure and physical properties that are stable to about 1125 °C (transition temperature of β-wollastonite to α-wollastonite),[2] making wollastonite important in refractory ceramics production. Due to its needle-like morphology, thermal stability, low thermal expansion and low thermal conductivity, there is increasing demand for wollastonite as a substitute for short--fibre asbestos. Another boost to the industry came from its low dielectric constant and low dielectric loss at high frequency, making this material suitable for high frequency insulators.[3] In the production of plastics such as nylons, phenolic moulding compounds, polyesters, polyurethanes and polyureas, wollastonite is used as filler providing reinforcement, hardening, crack resistance, high brightness and other benefits.[4] In ceramics, wollastonite reduces warping and cracking and acts as a sintering aid which accelerates densification of ceramics and increases strength. In recent years, studies have reported improvements in strengths, shrinkage resistance and reduction in permeability for concrete mixes containing wollastonite as a cement replacement.[5] Moreover, several studies have examined wollastonite as an adsorbent for the removal of heavy metal ions, such as As^{+5} and Cr^{+6}, from water.[6]

Another high merit for wollastonite is its good bioactivity, biocompatibility, degradability and favourable mechanical characteristics. Consequently, it is increasingly being used as a biomaterial suitable for orthopaedic applications including medical material for bone substitution and dental roots. It should be emphasized that β-wollastonite phase has better bioactivity performance than α-wollastonite. Hence, β-wollastonite nanowires may be used as strength-enhancing additives for the preparation of the ceramics or bioactive nano-composites with improved mechanical properties.[3]

Biomaterials are generally defined as natural or man-made materials designed for use in the manufacturing of medical devices to replace a part or function of the biological system in a safe, reliable, economic and physiologically acceptable way. Although biomaterials are primarily intended for medical applications, there are also studies in which the term “biomaterials” refers to those materials produced by living organisms.[7]

According to the type of material used, biomaterials can be classified into one of four broad categories: metals, polymers, ceramics and composites. Among them, ceramic materials are very biocompatible and show exceptional wear resistance, but they are usually stiff and brittle. In order to improve the mechanical and textural characteristics of ceramics, new structures have to be created. Those structures may include, among others, ceramic composites with various fibres used as reinforcement. Moreover, calcium silicate based glass ceramics possess excellent

biocompatibility and bioactivity, and have been considered as potential candidates for bone replacement and regeneration.[8,9] Controlled crystallization of calcium silicate glass ceramics produces certain sodium calcium silicate phases, such as $Na_2Ca_2Si_3O_9$ which develop improved mechanical properties and enhanced stability of biomaterial under physiological conditions.[10] Also, there is a wide group of biomaterials developed for bone tissue engineering based on hydroxyapatite scaffolds.[11–13]

Needle-like bioceramics can be prepared by various techniques such as coprecipitation, sol–gel, sonochemical and hydrothermal methods. There are several studies reporting that wollastonite fibres can be obtained by calcination of tobermorite or xonotlite fibres as precursors above 800 °C. Hydrothermal process and hydrothermal microemulsion technique are also utilized to synthesize precursors for wollastonite fibres using small droplets of microemulsion as nanoreactors for the synthesis of nanoparticles with a low polydispersity.[3,14] However, microemulsion and soft template methods are limited by the large amount of template material required and the use of organic solvents and surfactants, which are dangerous pollutants. Autoclaving has been explored by Ismail *et al*. as a safe and environment-friendly technique for wollastonite synthesis.[15] However, all these techniques produce precursors that demand an additional sintering step to obtain *β*-wollastonite.[15]

Herein, we report the fabrication of needle-like wollastonite through a facile one-step hydrothermal method without any additional templates. The obtained product was employed for the bioactive composite production through a powder sintering route using bioglass as the matrix and needle-like wollastonite as the reinforcement. To study in detail the structure, morphology and sintering behaviour of the wollastonite and glass-ceramic composites, X-ray diffraction (XRD), adsorption–desorption isotherms of N_2 at –196 °C, scanning electron microscopy (SEM) equipped with EDX, FTIR and Raman spectroscopy methods were applied. *In vitro* bioactivity assessment of the composite and its potential as an implantable material was examined by immersion in simulated body fluid (SBF) at 37 °C for 21 days.

EXPERIMENTAL

Wollastonite synthesis

The procedure applied for the synthesis of wollastonite is as follows. The amount of 3.54 g $Ca(NO_3)_2{\cdot}4H_2O$ was dissolved in 35 ml of deionised water to obtain a clear solution. In a separate beaker, 3.18 g of $Na_2SiO_3{\cdot}5H_2O$ was dissolved in another 35 ml of deionised water and then dropped into $Ca(NO_3)_2$ stirred solution to obtain a milky-white suspension. The suspension was stirred for 30 min to ensure that the particles were well mixed and finely dispersed into the liquid. Subsequently, 10 ml of 5 M NaOH was added and stirring was continued for 5 min. The suspension was then transferred into a stainless steel autoclave and heated at 220 °C for 240 min at an autogenous pressure of 19 bar*, followed by cooling to room temperature naturally. After the hydrothermal reaction, the obtained suspension was filtered and washed

* 1 bar = 100 kPa

with deionised water three times. The resultant powder was dried at 105 °C for 3 h. This synthetic route is based on the following chemical reactions:

$$Ca(NO_3)_2 \rightleftharpoons Ca^{2+} + 2NO_3^- \quad (1)$$

$$Na_2SiO_3 \rightleftharpoons 2Na^+ + SiO_3^{2-} \quad (2)$$

$$Ca(NO_3)_2 \cdot H_2O + Na_2SiO_3 \cdot 5H_2O \rightleftharpoons CaSiO_3 \cdot H_2O + 2NaNO_3 + 5H_2O \quad (3)$$

Bioglass synthesis

During the synthesis, a specific melting regime of SiO_2, Na_2CO_3, P_2O_5 and $CaCO_3$ was applied in order to obtain a composition given by the mass fraction of oxides: 45 wt. % SiO_2, 24.5 wt. % CaO, 24.5 wt. % Na_2O and 6.0 wt. % P_2O_5. The melting regime in a platinum crucible included heating at 1000 °C for 15 min, then heating at 1100 °C for 15 min with maintaining that temperature for the next hour. After that time, the procedure continued by heating up to 1200 °C for 15 min and keeping that temperature for another hour. The melted mass was poured onto a metal plate heated to 380 °C and allowed to cool. After cooling, the glass was crushed in an agate mortar and pulverized by grinding in a ball mill. The powder was passed through a sieve of 180 mesh.

Composite fabrication

The glass–ceramics composites were fabricated by sintering pellets (Ø 15 mm), which were previously prepared from the wollastonite and glass powder in a mass ratio of 1:4 (0.1 g + 0.4 g) by cold pressing in a laboratory hydraulic press. Components were well mixed in an ethanol suspension through sonication. Then polyvinyl alcohol (PVA) solution was added to achieve agglomeration of particles. The obtained precipitate was dried, powdered in an agate mortar and pressed in a laboratory hydraulic press at 10 t. The temperature of sintering was selected to be 1000 °C, according to our preliminary findings. The samples were heated at the chosen temperature for 15, 30, 55 and 85 min, initially cooled down to 300 °C, and then to room temperature. After cooling, the sintered samples were subjected to subsequent analysis. Pure bioglass powder was sintered under the same conditions as the composite in order to compare their physicochemical properties and to more clearly demonstrate the influence of the wollastonite phase on the characteristics of the composite.

Characterization

The microstructures of the powder samples and composites substrates were analysed by scanning electron microscopy (SEM) using a JEOL JXA-8500F and a Leo Gemini 1530 by Zeiss with an Everhart-Thornley detector for collecting secondary electrons. The accelerating voltage was 10 kV.

Structural characteristics of crystal phases were examined by X-ray diffraction, using a STADI P instrument from STOE & Cie GmbH with a Mythen1K detector. CuKα radiation was used at 40 kV and 40 mA. The XRD technique was used to identify the phase composition of the bioglass, wollastonite, as well as sintered glass-ceramic composites. The diffraction data were collected in the 2θ Bragg angle range from 20 to 100°. The crystallite size of the wollastonite was calculated by the Scherrer equation with data obtained from the XRD analyses. This equation is given as:

$$L = \frac{K\lambda}{\beta \cos\theta} \quad (4)$$

where L is the crystallite size, K is the Scherrer constant, λ is the X-ray wavelength, β (expressed in radians) is the width of the peak (full width at half maximum – FWHM) after correction for

instrumental peak broadening and theta (θ) is the Bragg angle. The K value used in this calculation is 0.94. The quantification of individual crystalline phases in the samples was carried out based on the reference intensity ratio (RIR) method.

For textural analyses of wollastonite, Horiba SA-9601 MP BET surface area analyser and Thermo Scientific from Surfer were used. Experimental parameters for the N_2 adsorption/desorption analysis are presented in Supplementary material to this paper.

Additional structural characterization of the wollastonite samples was performed by Raman spectroscopy using a Raman Spectrometer Renishaw inVia 2 Raman microscope with applying a laser source with a wavelength of 532 nm. All FTIR absorption spectra were recorded in the wavenumber range from 400 to 4000 cm^{-1} (transmission mode) using a Bomem spectrometer. The resolution used was 4 cm^{-1} and the number of scans was 32.

In vitro *bioactivity assessment of the prepared glass–ceramics*

Simulated body fluid (SBF) has nearly the same ionic composition and pH value as blood plasma. SBF is used for *in vitro* testing and evaluation of the bioactivity of artificial materials by forming an apatite layer in the fluid. Additionally, it is used for the preparation of bioactive composites that will form bone-like apatite on various substrates. For SBF preparation, 750 ml of deionized water was poured into 1 L beaker and placed onto the heated magnetic stirrer with the temperature being maintained at 37 °C. Defined quantities of the following chemicals of the highest purity have been added slowly in small increments: 7.996 g NaCl, 0.35 g $NaHCO_3$, 0.224 g KCl, 0.228 g $K_2HPO_4{\cdot}3H_2O$, 0.305 g $MgCl_2{\cdot}6H_2O$, 40 ml 1 M HCl, 0.278 g $CaCl_2$, 0.071 g Na_2SO_4, 6.057 g Tris(hydroxymethyl)aminomethane (Tris) and a suitable volume of 1 M HCl for pH adjustments. Prepared solution was kept in a polyethylene bottle at 5–10 °C.

The glass–ceramic samples in the form of pellets were placed in polyethylene flasks containing 50 ml of simulated body fluid (SBF) in order to estimate their bioactivity. The covered flasks were kept at 37 °C for 21 days. Subsequently, the samples were removed from the SBF solution, washed with distilled water and then air-dried at room temperature. The sample was examined by an XRD analysis of the powdered glass-ceramic samples

RESULTS AND DISCUSSION

SEM

Wollastonite morphology analysed by SEM along with element mapping and distribution of the main elements are given in Fig. 1. Needle-like wollastonite particles with length up to 25 μm and very sharp ends can be noticed in Fig. 1a and b. In addition, it can be observed that larger particles are composed of aggregation and stacking of smaller ones which form broom-shaped structures at the ends. Fig. 1c–e show element mapping and distribution of the main elements in the wollastonite. EDX analysis of needles, shown in Fig. 1k, confirmed the ternary system of the wollastonite, containing the elements silicon, calcium and oxygen. However, sodium is also present in the structure probably due to its adsorption on the surface from the reaction mixture during autoclaving. Peaks for C and Pt originate from sputtered platinum and carbon which served as coating material used to coat non-conductive wollastonite samples for standard SEM observations.

From the SEM image of the calcined powder (Fig. 1f and g), it can be seen that the original shapes and sizes of wollastonite were predominantly preserved,

but a sintering process occurred giving morphologies which could be described as needles of different sizes between 2 and 20 μm in length. The edges and ends of needles are rounded and this is probably the result of surface melting of particles due to the presence of sodium on the surface which acts as a flux. Such behaviour of wollastonite at the calcination temperature could be exploited well to provide strong adhesion between wollastonite reinforcement and the glass matrix during preparation of the composite. Fig. 1h–j show element mapping of calcined wollastonite. The additional micrographs of the wollastonite at different magnifications are provided in Supplementary material (Figs. S-1 and S-2).

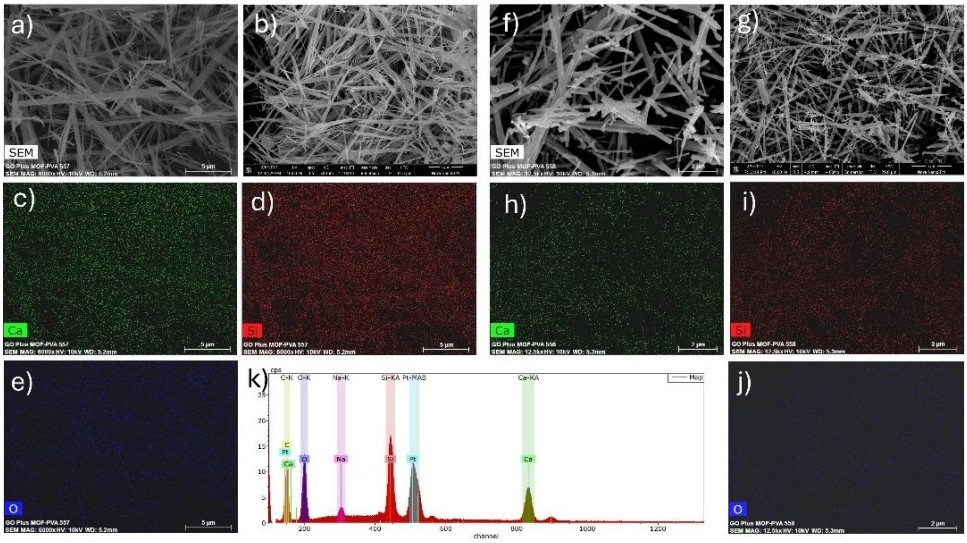

Fig. 1. SEM images of needle-shaped wollastonite along with element mapping and distribution of the main elements; a) and b) as-synthesized wollastonite and distribution of: c) Ca, d) Si, e) O, f) and g) calcined wollastonite and distribution of: h) Ca, i) Si, j) Si, k) EDX analysis of as-synthesized wollastonite.

XRD

X-ray diffraction patterns of the as-synthesized wollastonite and wollastonite after its calcination at 900 °C for 2 h are shown in Fig. 2. The observed diffraction peaks of the XRD patterns could be indexed as monoclinic wollastonite (β-$CaSiO_3$) with space group of $P2_1/a$ (PDF 00-066-0271). The geometry of the unit cell is defined by the following parameters: approximately a = 15.43 Å, b = 7.33 Å, c = 7.07 Å and angles α = 90.00°, β = 95.31°, γ = 90.00°.

The position, intensities and shape of the strong diffraction peaks for the calcined sample of wollastonite coincide well to the standard values and imply that it was better crystallized than that of as-synthesized sample. Table S-I of the Supplementary material shows the positions (2θ) of the peaks, interplanar d-spacings, full

width at half maximum (*FWHM*), background intensity and areas of the peaks collected from the XRD pattern (Fig. 2). The effect of autoclaving and subsequent calcination on the crystallite size and micro strain of the *β*-wollastonite was calculated with data from the XRD analysis and also shown in Supplementary material (Table S-I). The results indicate an increase in average crystallite size after calcination from 46.3 to 48.6 nm, while micro strain was reduced from 0.340 to 0.234 indicating improved crystallinity and reduced internal defects. The peaks observed at 23.2, 25.3, 26.8, 28.9, 30.0, 36.2, 39.04, 41.3, 50.9 and 53.05° correspond to the (400), (002), (–202), (202), (–320), (412), (–422), (040), (004) and (523) planes.

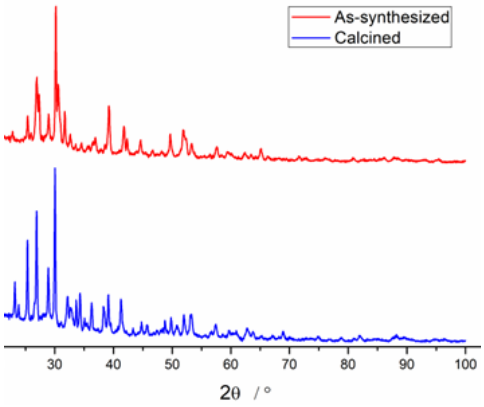

Fig. 2. XRD patterns of as-synthesized wollastonite and calcined sample at 900 °C.

BET analysis

The N_2 adsorption–desorption isotherm and the Barrett–Joyner–Halenda (BJH) pore size distribution for the as-synthesized sample of wollastonite are plotted in Fig. 3a and b, respectively. The specific surface areas as obtained by the BET method, BJH adsorption cumulative surface area of pores, BJH total pore volume and BJH average pore diameter are listed in Table S-II of the Supplementary material.

The surface area of the wollastonite ceramics was measured to be 26 $m^2\ g^{-1}$. The single-point adsorption total pore volume for pores with a diameter less than 1.038 nm at $p/p° = 0.01$ was found to be 0.006 $cm^3\ g^{-1}$. The average pore diameters from BJH adsorption and desorption measurements were 6.1 and 6.3 nm, respectively.

As can be seen in Fig. 3a, as-synthesized wollastonite sample showed an unusual type III isotherm pattern which is convex to the $p/p°$ axis over its entire range. The isotherm does not exhibit a point B, but a very narrow hysteresis loop can be observed. This indicates that the adsorbent-adsorbate interaction is weak as compared with the adsorbate–adsorbate interactions.

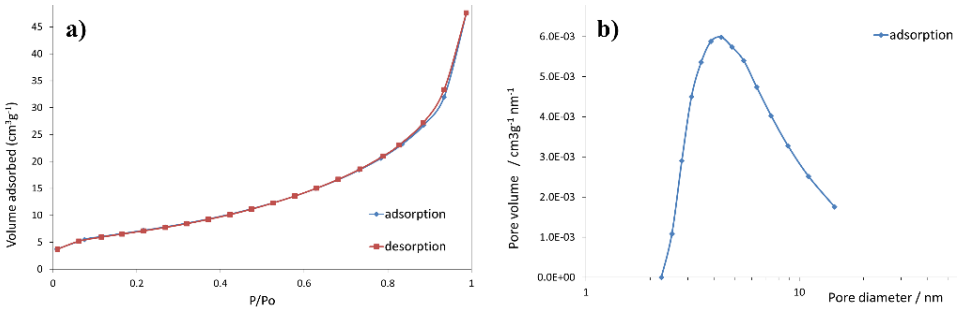

Fig. 3. a) The N_2 adsorption–desorption isotherm and b) BJH adsorption pore distribution of as-synthesized wollastonite sample.

Raman spectroscopy

The Raman spectra of as-synthesized and calcined wollastonite samples over the 100–1200 cm^{-1} spectral range are shown in Fig. 4. This figure shows the position and relative intensity of the Raman bands that originate from an unoriented sample of wollastonite. The most intense Raman bands, listed in order of increasing wavenumber at 330, 404, 580, 636, 860, 971 and 1042 cm^{-1}, align well with the *β*-wollastonite (2M) phase. The low-frequency bands occurring below 500 cm^{-1} are attributed to Ca–O stretching and Si–O bending modes. The prominent bands around 636, 860, 971 and 1042 cm^{-1} are associated with the Si–O–Si and O–Si–O vibrational stretching modes in the SiO_4 tetrahedron.[16,17] The comparative overview of the positions of Raman bands for native and calcined wollastonite is provided in Table S-III of the Supplementary material. The observed redshift in Raman peaks after calcination at 900 °C is attributed to lattice relaxation, reduced internal strain, and increased crystallite size, as confirmed by XRD analysis.

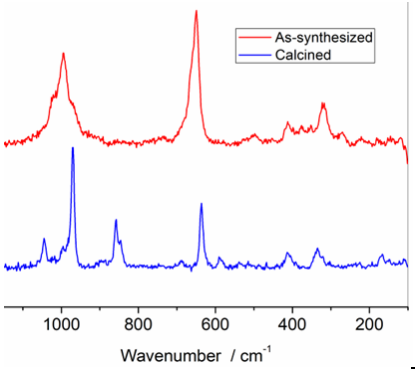

Fig. 4. Raman spectra of as-synthesized wollastonite and wollastonite after calcination at 900 °C.

FTIR spectroscopy

The FTIR spectra were used to analyse the structures of the wollastonite, as illustrated in Fig. 5. The most prominent bands are observed in the range from 850

to 1200 cm^{-1} and correspond to the vibrational modes of the asymmetric SiO_4 tetrahedron. Based on literature, the bands detected at 1087 and 1028 cm^{-1} correspond to stretching vibrations of bridging Si–O–Si, while those at 971 and 930 cm^{-1} are associated with non-bridging oxygen (Si–O) bonds.[18]

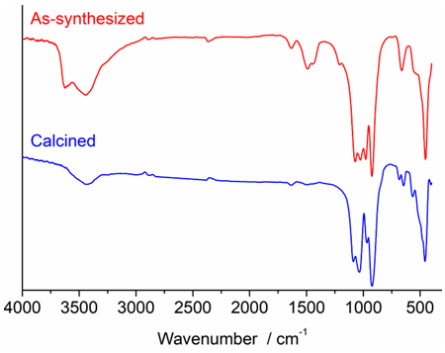

Fig. 5. FTIR spectra of as-synthesized wollastonite and wollastonite calcined at 900 °C.

The presence of Si–O–Ca non-bridging oxygen bonds was confirmed by the FTIR spectra of the fired powder, which exhibited vibrational modes at 903 cm^{-1}. These stretching vibrations of Si–O–Ca bonds indicate the formation of β–$CaSiO_3$ which is consistent with the obtained XRD patterns. Furthermore, the band peaking at 846 cm^{-1} is associated with Si–O–Ca vibrations, while the bands at 682 and 648 cm^{-1} reflect the symmetric stretching vibrations of Si–O–Si bonds. The bending vibrations of Si–O–Si bonds are detected around 567 and 452 cm^{-1}. It is important to note that many peaks in the spectrum overlap, making it challenging to identify specific bonds unambiguously.

The significant difference in the spectra was observed only in the 3625, 1490 and 1449 cm^{-1} peaks. The last two bands were ascribed to the carbonate group. The bands at 3625 and 3438 cm^{-1} were evidence of O–H stretching vibration of the structural –OH groups and absorbed water, respectively. The band at 1637 cm^{-1} is associated with O–H bending vibration. Calcination of the sample caused decomposition of carbonates and removal of structural –OH groups.[19,20]

Composite characterization

To highlight the influence of wollastonite on the sintering behaviour and physicochemical properties of the composites, a comparative analysis of sintered materials based on pure bioglass and wollastonite–bioglass composites is presented. Sintered samples of pure bioglass (BG) (Figs. S-3–S-6 of the Supplementary material), obtained at the same temperature but with different sintering times, exhibit a very broad pore size distribution, ranging from several nm up to 100 μm, indicating a diverse range of pore sizes within their structure. This characteristic can significantly influence its adsorption properties and overall performance in biomedical applications. The specific surface area of the material is less than 1 m^2

g^{-1}, suggesting a relatively low surface area compared to other materials. Additionally, the pore volume (V_p) is within the range of 0.036–0.055 cm^3 g^{-1} and the highest measured porosity of the sintered bioglass is 10.7 %. (depending on sintering time), indicating a limited capacity for storing fluids. The predominant mineral in the composition of the samples is combeite, which comprises between 96 and 100 % of the material. This percentage increases with the duration of sintering. The SEM micrographs presented in Figs. S-3–S-6 indicate surface melting of the material, particle coalescence through the formation of so-called necks, and the development of globular and rounded particle morphologies.

Fig. 6a and Fig. S-7 (Supplementary material) show SEM micrograph of the composite treated at 1000 °C for 15 min (COM 15). There are clear signs indicating the onset of the sintering process, characterized by the formation of interparticle contacts, commonly referred to as necks, which are established between the particles through weak cohesive forces. The chemical composition of the composite obtained using the EDX method indicates that the amount of sodium is about 12 %, which acts herein as a flux and facilitates the consolidation of the composite during the heat treatment. Crystallographic analysis indicates that the dominant mineral is combeite $Na_2Ca_2Si_3O_9$ (98 %), the presence of which increases the mechanical strength of the material while maintaining its biocompatibility. Sodium calcium silicate which is also known in the literature as a bioactive material was also detected in the composite, with a mass fraction of several percent. The specific surface area is less than 1 m^2 g^{-1}, the porosity is 21 %, while the average pore diameter is 4256 nm. These results confirm that the sintering process is in the initial phase, so that there has not yet been significant densification of the material and elimination of porosity.

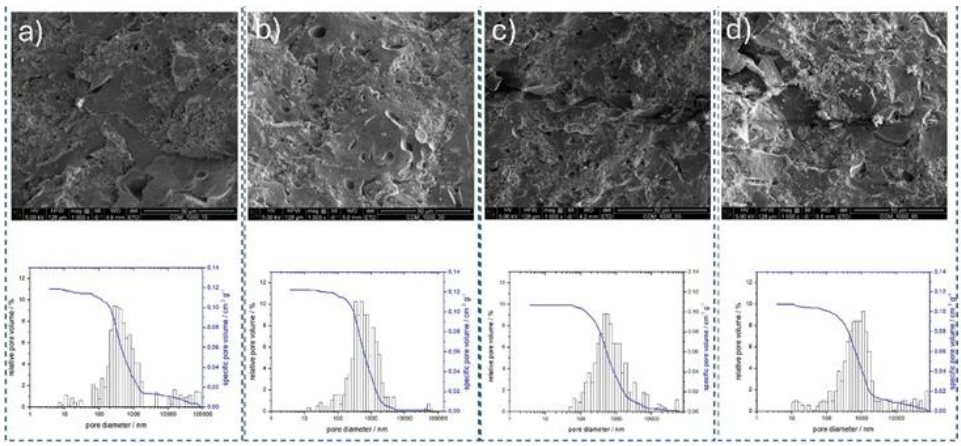

Fig. 6. SEM micrographs and pore size distributions of the composite treated at 1000 °C for: a) 15 (COM 15), b) 30 (COM 30), c) 55 (COM 55) and d) 85 min (COM 85).

Fig. 6b and Fig. S-8 (Supplementary material) show micrographs of the composite surface after 30 min of sintering (COM 30). At this stage, the presence of large, consolidated particles that were formed during the process is observed, as well as the presence of smaller particles with an elongated morphology that indicate that sintering has not been completed yet. Despite this, the data obtained by nitrogen adsorption/desorption indicated that the porosity remained the same (21%), but a decrease in the mean pore diameter was noted, which changed to 1368 nm. The mass fraction of combeite has been shown to be at the level of the previous sample (98 %).

After calcination for 55 min (COM 55), no significant changes in the surface morphology of the composite were recorded, as can be seen in Fig. 6c and Fig. S-9 (Supplementary material). The porosity has been shown to be 19 % with the mean pore diameter of 1956 nm. The chemical changes that occur during thermal treatment led to the complete dominance of combeite minerals, whose mass fraction turned to 99.5 %. The last sample was sintered for 85 min (COM 85), and its surface morphology can be seen in Fig. 6d and Fig. S-10 (Supplementary material). In the figures, elongated particles of worm-like morphology, like spaghetti, can no longer be observed, as was the case with the previous samples. Based on morphology, it can be concluded that this is the final stage of sintering. The pore volume did not change significantly, but there was an increase in the mean pore diameter to a value of about 3928 nm. Therefore, during sintering and the formation of the liquid phase at a given temperature, the smaller pores were filled, or they joined each other into pores with a larger diameter. It should be kept in mind that sintering did not take place under high pressure. Generally, the composites typically exhibit a higher pore volume (V_p) of up to 0.122 $cm^3\ g^{-1}$ and a narrower pore size distribution compared to sintered bioglass. These properties enhance their performance and suitability in the field of biomedical engineering.

Interaction of bioactive composite COM 30 with SBF

To test the interaction of the bioactive composite with SBF, the COM 30 sample was used, as the sintering time of 30 min had been established as optimal for obtaining a mechanically stable material. After interaction with the solution, some changes were observed in the XRD diffractogram. This suggests that the crystal structure of the material remained largely unchanged, except for the appearance of small peaks associated with hydroxyapatite formation, which were just above the detection limits of the XRD method (Fig. S-11 of the Supplementary material). This result aligns with findings from other studies, as the phosphate content in SBF relative to the mass of the composite sample is minimal resulting in sparsely distributed apatite precipitates.

CONCLUSION

This study demonstrated a robust approach to the synthesis of β-wollastonite microfibres through a simple, template-free hydrothermal technique, followed by calcination at 900 °C to improve crystallinity and eliminate constitutional water. The resultant β-wollastonite exhibited a needle-like morphology with high mesoporosity and surface area, as confirmed by SEM, XRD and BET analyses. These characteristics were favourable for enhancing the structural and bioactive properties of the composite material.

The wollastonite microfibres were successfully employed as a constituent in a glass-ceramic composite, which was prepared by a powder sintering method using bioglass as the matrix. The addition of wollastonite contributed to the formation of sodium-calcium-silicate phases (mostly combeite), which improved the mechanical properties of the composite while maintaining its biocompatibility.

The calcination and sintering processes facilitated the consolidation and densification of the composite, supported neck formation between particles and led to the development of appropriate porosity suitable for the intended application. XRD analysis confirmed the dominant β-wollastonite phase with improved crystallite size and reduced microstrain post-calcination, contributing to the composite's structural stability and bioactivity. Overall, the *in vitro* bioactivity assessment in simulated body fluid highlighted the composite's potential for its use as a bioactive implant material, with surface changes suggesting the formation of bioactive phases, though further studies are needed to optimize hydroxyapatite formation.

SUPPLEMENTARY MATERIAL

Additional data and information are available electronically at the pages of journal website: https://www.shd-pub.org.rs/index.php/JSCS/article/view/13354, or from the corresponding author on request.

Acknowledgement. This work was funded by the Ministry of Science, Technological Development and Innovation of the Republic of Serbia (Agreement number 451-03-137/2025-03/ /200124).

ИЗВОД

РАЗВОЈ СТАКЛО-КЕРАМИЧКОГ КОМПОЗИТА ОЈАЧАНОГ β-ВОЛАСТОНИТОМ СИНТЕТИСАНИМ ХИДРОТЕРМАЛНОМ МЕТОДОМ

МАРЈАН РАНЂЕЛОВИЋ[1], CHARLES C. SORRELL[2], SHARON КОРРКА[3], АЛЕКСАНДРА ЗАРУБИЦА[1], МИЛАН З. МОМЧИЛОВИЋ[1] и DIRK ENKE[3]

[1]Универзитет у Нишу, Природно–математички факултет, Департман за хемију, Вишеградска 33, 18000 Ниш, [2]2School of Materials Science and Engineering, University of New South Wales, Sydney NSW 2052, Australia и [3]Institute of Chemical Technology, University of Leipzig, Linne str. 3, 04103 Leipzig, Germany

Микровлакна β-воластонита (β-$CaSiO_3$) су успешно синтетисана применом једностепене хидротермалне реакције без употребе темплејта, коришћењем калцијум-нитрата и натријум-метасиликата у алкалној средини. Синтеза је изведена на температури од 220

°C за само 240 min под аутогеним притиском од 19 bar. Овим поступком избегава се формирање ксонотлита као интермедијарне фазе, чиме се елиминише потреба за накнадном калцинацијом у циљу добијања воластонита. Рендгенска дифракција (XRD) је потврдила присуство фазе *β*-воластонита, док су анализе након калцинације указале на побољшану кристаличност и структурне карактеристике. Скенирајућа електронска микроскопија (SEM) је открила морфологију у облику иглица, а анализа адсорпције–десорпције азота је показала развијену специфичну површину од 26 $m^2 g^{-1}$ и изражену мезопорозност. Ове повољне карактеристике омогућиле су интеграцију *β*-воластонита у синтези стакло–керамичког композита, који је потом карактерисан у погледу морфолошких, структурних, текстурних и *in vitro* биоактивних својстава. Композит је припремљен мешањем прахова *β*-воластонита и биоактивног стакла у масеном односу 1:4, након чега је уследило компактирање једноосним пресовањем и синтеровање на 1000 °C у различитим временским интервалима. Ради поређења, компактне пастиле чистог биостакла такође су синтероване под истим условима. Структурна, морфолошка, текстурална и *in vitro* биоактивна карактеризација показала је да је додавање *β*-воластонита довело је до уједначеније и уже расподеле величина пора и подстакло формирање веза (вратова) између честица, указујући на потенцијал композита за примену у регенерацији костију.

(Примљено 26. априла, ревидирано 20. маја, прихваћено 25. августа 2025)

REFERENCES

1. C. C. Lin, P. Shen, *Mater. Chem. Phys.* **182** (2016) 508 (https://doi.org/10.1016/j.matchemphys.2016.07.065)
2. E. Mazzucato, A. F. Gualtieri, *Phys. Chem. Miner.* **27** (2000) 565 (https://doi.org/10.1007/s002690000095)
3. K. Lin, J. Chang, G. Chen, M. Ruan, C. Ning, *J. Cryst. Growth* **300** (2007) 267 (https://doi.org/10.1016/j.jcrysgro.2006.11.215)
4. K. Lin, C. Lin, Y. Zeng, *RSC Adv.* **6** (2016) 13867 (https://doi.org/10.1039/c5ra26916d)
5. M. A. Abdelwahab, *A Reflexive Reading of Urban Space*, 1st ed., eBook ISBN 9781315565125, Taylor and Francis, London, 2018
6. N. Obradović, S. Filipović, S. Marković, M. Mitrić, J. Rusmirović, A. Marinković, V. Antić, V. Pavlović, *Ceram. Int.* **43** (2017) 7461 (https://doi.org/10.1016/j.ceramint.2017.03.021)
7. W. K. Lam, J. C. Y. Leong, Y. H. Li, Y. Hu, W. W. Lu, *Gait Posture* **22** (2005) 189 (https://doi.org/10.1016/j.gaitpost.2004.09.011)
8. V. S. Topalović, S. R. Grujić, V. D. Živanović, S. D. Matijašević, J. D. Nikolić, J. N. Stojanović, S. V. Smiljanić, *Ceram. Int.* **43** (2017) 12061 (https://doi.org/10.1016/j.ceramint.2017.06.061)
9. M. Riaz, R. Zia, A. Mirza, T. Hussain, F. Bashir, S. Anjum, *Mater. Sci. Eng., C* **75** (2017) 872 (https://doi.org/10.1016/j.msec.2017.02.141)
10. L. Adams, E. R. Essien, R. O. Shaibu, A. Oki, *New J. Glass Ceram.* **3** (2013) 11 (http://dx.doi.org/10.4236/njgc.2013.31003)
11. A. Logeshwaran, R. Elsen, S. Nayak, *J. Mech. Behav. Biomed. Mater.* **138** (2023) 105633 (https://doi.org/10.1016/j.jmbbm.2022.105633)
12. A. Iatsenko, O. Sych, A. Nikolenko, S. Stelmakh, *Results Surf. Interfaces.* **16** (2024) 100265 (https://doi.org/10.1016/j.rsurfi.2024.100265)
13. I. W. Suh, S. R. Jang, E. M. Hia, C. H. Park, C. S. Kim, *Mater. Chem. Phys.* **326** (2024) 129865 (https://doi.org/10.1016/j.matchemphys.2024.129865)

14. E. Zeimaran, S. Pourshahrestani, S. F .S. Shirazi, B. Pingguan-Murphy, N. A. Kadri, M.R. Towler, *J. Non-Cryst. Solids* **443** (2016) 118 (https://doi.org/10.1016/j.jnoncrysol.2016.04.005)
15. H. Ismail, R. Shamsudin, M. A. A. Hamid, *Mater. Sci. Eng., C* **58** (2016) 1077 (https://doi.org/10.1016/j.msec.2015.09.030)
16. B. Chaudhary, Y.K. Kshetri, D.R. Dhakal, S. W. Lee, T. H. Kim, *Opt. Mater.* **135** (2023) 113326 (https://doi.org/10.1016/j.optmat.2022.113326)
17. J. Zhu, T. Qu, S. Niu, J. Liu, S. Liu, J. Geng, Z. Yang, A. Abulizi, *Mater. Today Sustain.* **26** (2024) 100716 (https://doi.org/10.1016/j.mtsust.2024.100716)
18. A. Sobhani, E. Salimi, *Ceram. Int.* **50** (2024) 26869 (https://doi.org/10.1016/j.ceramint.2024.04.417)
19. S. Palakurthy, S. Patel, K. V. Reddy, R. Samudrala, C. Padala, B. Manavathi, P. A. Azeem, *Ceram. Int.* **49** (2023) 36344 (https://doi.org/10.1016/j.ceramint.2023.08.318)
20. C. Paluszkiewicz, M. Blażewicz, J. Podporska, T. Gumuła, *Vibr. Spectrosc*. **48** (2008) 263 (https://doi.org/10.1016/j.vibspec.2008.02.020).